Magnetic cycles in global large eddy simulations of solar convection

Mihai Ghizaru*, Paul Charbonneau*, Piotr K. Smolarkiewicz**
*Département de Physique, Université de Montréal,
C.P. 6128 Succ. Centre-ville, Montréal, Qc, H3C-3J7 CANADA
**National Center for Atmospheric Research, Boulder, CO 80307, USA

ABSTRACT

We report on a global magnetohydrodynamical simulation of the solar convection zone, which succeeds in generating a large-scale axisymmetric magnetic component, antisymmetric about the equatorial plane and undergoing regular polarity reversals on decadal timescales. We focus on a specific simulation run covering 175 yr, during which 5 polarity reversals are observed, with a mean period of 32 yr. Time-latitude slices of the zonally-averaged toroidal magnetic component at the base of the convecting envelope show a well-organized toroidal flux system building up in each solar hemisphere, peaking at mid-latitudes and migrating towards the equator in the course of each cycle, in remarkable agreement with inferences based on the sunspot butterfly diagram. The simulation also produces a large-scale dipole moment, varying in phase with the internal toroidal component, suggesting that the simulation may be operating as what is known in mean-field theory as an $\alpha\Omega$ dynamo.

Subject headings: Convection — MHD — Sun: magnetic fields — Sun: cycle

1. Numerical simulations of convection and the solar dynamo

It is now generally agreed upon that the solar activity cycle ultimately owes its existence to the inductive action of fluid flows pervading the solar interior; cf. Charbonneau (2005). In view of the physical conditions therein, the associated dynamo mechanism is believed to be well-described by the MHD equations — cf., Priest 2000, Goedbloed and Poedts 2004 — but the turbulent nature of these internal flows yields a computationally challenging problem. Gilman (1983) and Glatzmaier (1984, 1985) produced the first large-scale numerical simulations resulting in cyclic dynamo action in the solar convection zone, but in view of computing limitations their groundbreaking simulations operated in physical parameter regime rather far removed from solar interior conditions. Following the advent of high-performance computing, parallelized versions of the Glatzmaier simulation model (Clune *et al.* 1999) made possible much higher resolution runs attaining a strongly turbulent regime (Miesch *et al.* 2000). Dynamo action in these simulations proved very efficient at producing small-scale magnetic fields, but failed to generate a spatially well-organized large-scale component, let alone equatorward migration and polarity reversals (Brun *et al.* 2004). Further simulations showed that towards this end the presence of a stably stratified tachocline-like layer, where significant rotational shear could persist, allowed the buildup of a strong, large-scale magnetic component, antisymmetric about the equator and persistent on yearly timescales (Browning *et al.* 2006). However, no polarity reversals were observed over the 8 yr time span of these simulations[1].

Herein, we report on a series of global MHD simulations of the solar convection zone (SCZ), conceptually similar to those referenced above,

[1]M.K. Browning (personal communication) informs us that subsequent to the publication of the Browning *et al.* (2006) paper their simulations were extended to 30 years, still without producing any hint of polarity reversal.

that do produce well-organized large-scale magnetic fields undergoing regular cyclic polarity reversals on decadal timescales.

2. Model formulation

Our global model integrates the anelastic form of the MHD equations (Glatzmaier 1984) in a thick, rotating spherical shell of electrically conducting fluid. We use a modified version of the general-purpose hydrodynamical simulation code EULAG (cf. Prusa et al 2008 for a review) in which we have introduced magnetic fields and a solar-like stratification of the ambient state. Our overall simulation setup is similar to that in Browning *et al.* (2006). The solution domain spans the range $0.61 \leq r/R_\odot \leq 0.96$, covering 3.4 density scale heights and across which we force the solar heat flux. The background stratification is convectively stable in the bottom portion of the domain ($0.61 \leq r/R_\odot \leq 0.71$), and unstable above. Stress-free boundary conditions are imposed at the top and bottom boundaries, with the magnetic field set to zero at the bottom (perfect conductor) and constrained to remain radial at the top (magnetically open). We defer an exposition of the model formulation to a forthcoming publication, with only a few highlights provided below.

The anelastic hydrodynamic SCZ model of Elliot & Smolarkiewicz (2002) is cast in an anholonomic time-dependent curvilinear framework of Prusa & Smolarkiewicz (2003), which enables mesh adaptivity, and extended to MHD. The governing equations take the form:

$$\begin{aligned}
\frac{D\mathbf{v}}{Dt} &= -\nabla\pi - \mathbf{g}\frac{\theta'}{\theta_o} + 2\mathbf{v}'\times\boldsymbol{\Omega} + \frac{1}{\mu\rho_o}\left(\mathbf{B}\cdot\nabla\right)\mathbf{B} + \mathcal{D}_\mathbf{v} \ , \\
\frac{D\theta'}{Dt} &= -\mathbf{v}\cdot\nabla\theta_e + \mathcal{H} - \alpha\theta' \ , \\
\frac{D\mathbf{B}}{Dt} &= -\nabla\pi^* + \left(\mathbf{B}\cdot\nabla\right)\mathbf{v} - \mathbf{B}(\nabla\cdot\mathbf{v}) + \mathcal{D}_\mathbf{B} \ , \\
\nabla\cdot(\rho_o\mathbf{v}) &= 0 \ , \quad \nabla\cdot\mathbf{B} = 0 \ ,
\end{aligned} \tag{1}$$

where $\mathbf{v}$ and $\mathbf{B}$ denote vectors of the physical velocity and of the magnetic field, measurable at every point of the spherical shell in a local Cartesian frame tangent to the lower surface of the shell, and θ is the potential temperature (tantamount to the specific entropy, $s = c_p \ln\theta$). Subscripts "o " refer to the basic isentropic state with density satisfying hydrostatic balance with radially decreasing gravity. Primes denote deviations from an arbitrary prescribed ambient state (which can, but does not have to, coincide with the basic state; Prusa et al. 2008). In the momentum equation, π is a density-normalized pressure perturbation inclusive of the magnetic pressure and centrifugal force, and $\mathcal{D}_\mathbf{v}$ symbolizes viscous dissipation. In the entropy equation, $\mathcal{H}$ combines heat sink/sources due to radiation, diffusion and viscous heating. The Newtonian relaxation term, with an inverse time-scale α, forces the system towards an ambient stable/unstable thermodynamic profile in the tachocline/SCZ. In the induction equation, the gradient of potential π^* denotes an auxiliary term introduced to assure $\nabla\cdot\mathbf{B} = 0$ in numerical integrations, and $\mathcal{D}_\mathbf{B}$ is a short hand for magnetic diffusion. All other symbols have their usual meaning. Using the mass continuity equation and the $\mathbf{B}$ solenoidality constrain, the system (1) is rewritten as a set of Eulerian conservation laws and solved using the non-oscillatory forward-in-time (NFT) approach, widely documented in the literature; cf. Prusa et al. 2008 and Smolarkiewicz & Szmelter (2009) for recent reviews and discussions. In essence, the resulting system of PDE is viewed as

$$\frac{\partial\rho^*\boldsymbol{\Psi}}{\partial t} + \nabla\cdot\left(\mathbf{V}^*\boldsymbol{\Psi}\right) = \mathbf{R} \ , \tag{2}$$

where $\boldsymbol{\Psi}$ denotes the vector of prognosed dependent variables (components of $\mathbf{v}$, $\mathbf{B}$ and θ'), $\rho^* = G\rho_o$ combines the anelastic density and the Jacobian of coordinate transformation, $\mathbf{V}^* = \rho^*\dot{\mathbf{x}}$ is an effective transporting momentum with $\dot{\mathbf{x}}$ symbolizing the contravariant velocity of the actual curvilinear coordinates, and $\mathbf{R}$ is a shorthand for the associated right-hand-side (rhs) inclusive of the metric forces (viz. Christophel's terms). The model algorithm for a discrete integration of (2) in the time-space continuum relies on the implicit trapezoidal rule approximation. It is formulated in the spirit of

$$\boldsymbol{\Psi}_\mathbf{i}^{n,\nu} = \widehat{\boldsymbol{\Psi}}_\mathbf{i} + \frac{\delta t}{2}\mathbf{L}\boldsymbol{\Psi}\big|_\mathbf{i}^{n,\nu} + \frac{\delta t}{2}\mathbf{N}\boldsymbol{\Psi}\big|_\mathbf{i}^{n,\nu-1} - \nabla\boldsymbol{\Phi}\big|_\mathbf{i}^{n,\nu} \ , \tag{3}$$

with $n, \mathbf{i}$ and δt marking discrete locations in the model $(t, \mathbf{x})$ domain and a temporal increment, $\mathbf{L}$ and $\mathbf{N}$ denoting linear and nonlinear part of the rhs operators, $\boldsymbol{\Psi} \equiv (\mathbf{v},\ \theta',\ \mathbf{B})$, $\boldsymbol{\Phi} \equiv$

$0.5\delta t(\phi,\phi,\phi,0,\phi^*,\phi^*,\phi^*)$, and $\nu = 1,..,m$ numbering the fixed point iterations. With all prognostic dependent variables co-located, the execution of (3) invokes its local algebraic inversion with respect to $\mathbf{\Psi}_\mathbf{i}^{n,\nu}$; after which, enforcing discretized mass continuity and magnetic-field solenoidality on the components $\mathbf{v}$ and $\mathbf{B}$ leads to the associated discrete elliptic problems for ϕ and ϕ^*. These are solved with a robust, preconditioned non-symmetric Krylov-subspace solver (Smolarkiewicz et al., 1997, 2004), essentially completing the model algorithm. A key element of the NFT approach implemented in EULAG is a universally second-order-accurate (in time and space) NFT advection operator MPDATA that forms the explicit element $\widehat{\mathbf{\Psi}}_\mathbf{i} \equiv \mathcal{A}_\mathbf{i}(\mathbf{\Psi}^{n-1} + 0.5\delta t\mathbf{R}^{n-1}, \widetilde{\mathbf{V}}^*)$ of (3), with $\mathcal{A}$ and $\widetilde{\mathbf{V}}^*$ denoting, respectively, the advection operator and a solenoidal $\mathcal{O}(\delta t^2)$ estimate of $\mathbf{V}^*$ at $t^{n-1/2}$. MPDATA is a finite-volume, high-resolution multi-pass (iterative) upwind scheme, already well reviewed in the literature; cf. Smolarkiewicz & Szmelter (2009), and references therein.

A particular feature of MPDATA important for the present study is its proven dissipative property mimicking the action of explicit subgrid-scale turbulence models where flow is under-resolved, while maximizing the effective Reynolds number; see Waite & Smolarkiewicz (2008) and Piotrowski et al. (2009), for relevant discussions and references. Such calculations relying on the properties of non-oscillatory differencing are referred to in the literature as implicit large-eddy simulations, or ILES. In the experiments reported here, we retained only the radiative diffusion in the $\mathcal{H}$ forcing term on the rhs of the entropy equation in (1), while delegating the entire system dissipativity to ILES. Moreover, we use exclusively the third-order (for constant coefficients but second-order in general) option of MPDATA that minimizes the solution dependence on local Courant numbers while evincing desirable dissipative properties (Margolin and Smolarkiewicz 1998, Margolin et al. 2006).

3. Results: magnetic cycles

Figure 1 is a snapshot, in longitude-latitude Mollweide projection, of the radial component of the convective flow below the outer surface of the simulation domain. This flow exhibits the expected pattern of broad upflows cells (orange-yellow-white) delineated by a network of narrower downflow lanes (purple-blue-black), typical of thermal convection in a stratified environment (compare to Miesch *et al.* 2000, Fig. 5, and Brun *et al.* 2004, Fig. 1). The influence of rotation on convection is most pronounced in the equatorial regions, where convective cells become elongated and aligned in the latitudinal direction.

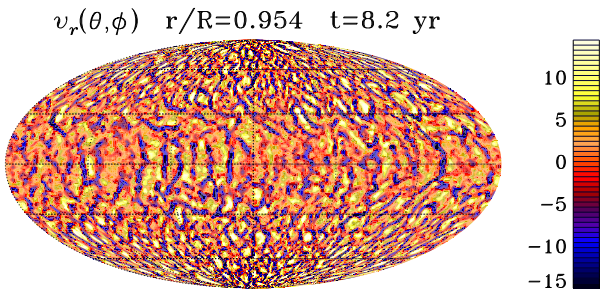

Fig. 1.— Radial component of the flow velocity at $r/R_\odot = 0.954$, near the domain top, in a $256 \times 128 \times 93$ simulation. The results are plotted in a Mollweide projection, with the color scale coding the flow speed in m s^{-1}. Peak radial flow speed occur in downflow lanes, and here can reach $\sim 25\,\mathrm{m\ s^{-1}}$.

In these surface and subsurface layers, the magnetic field is temporally and spatially intermittent, reaching locally values in excess of 0.1 T, but carries little net flux — the hallmark signature of turbulent small-scale dynamo action (Cattaneo 1999). The magnetic fields remains largely unstructured throughout the convective envelope, but at and below its base a strong and spatially well-organized large-scale component builds up. This occurs via the combined action of downward turbulent pumping of the magnetic field produced within the SCZ, amplification by the velocity shear present at the core-envelope interface, and reduced destruction of the field by the folding action of turbulence. The latter vanishes rapidly as one moves down into the tachocline-like stably stratified fluid layer underlying the SCZ. Figure 2 shows a snapshot of the toroidal magnetic component beneath the nominal interface between the bottom stable layer and the SCZ. Note that significant turbulence still persists at this depth, as a result

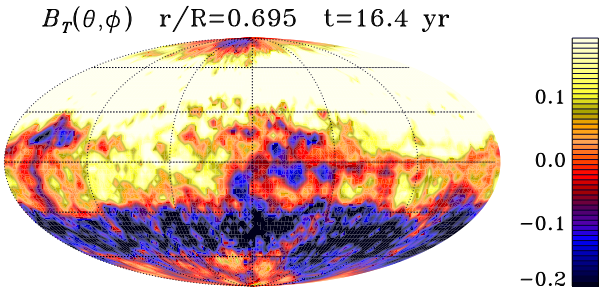

Fig. 2.— Toroidal component of the magnetic field, in the uppermost portion of the stable layer underlying the convective envelope ($r/R_\odot = 0.695$). A well-organized axisymmetric field component is evident, reaching 0.25 T in strength at mid-latitudes and showing antisymmetry about the equator. Although the snapshot is extracted in the nominally stable layer, convective undershoot from above induces strong fluctuations in the magnetic field.

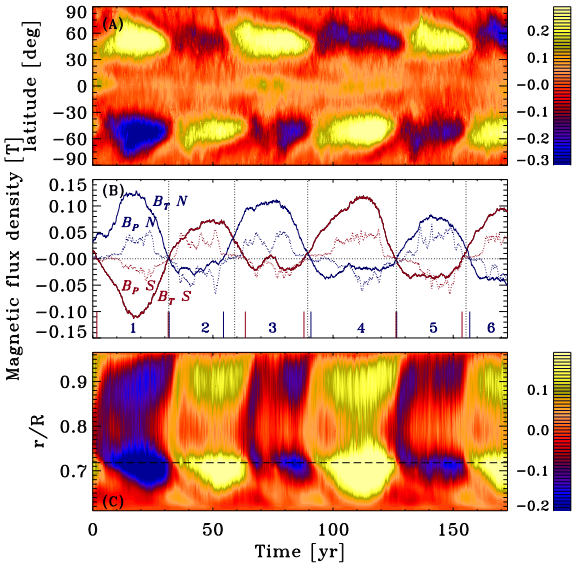

Fig. 3.— (A) Time-latitude "butterfly" diagram of the zonally-averaged toroidal magnetic field component at $r/R_\odot = 0.718$. (B) Time series of the hemispheric tachocline toroidal flux densities (solid lines) and polar cap radial magnetic flux densities (dotted lines). The vertical line segments indicate the time of polarity reversals of the deep-seated toroidal component for each hemisphere, as color-coded. (C) Time-radius slice of the zonally-averaged toroidal magnetic field component extracted at mid-latitudes in the Southern hemisphere. The base of the nominally unstable layer is indicated by a horizontal dashed line.

of convective undershoot from above, so that the magnetic field still shows strong local fluctuations. Yet, a very well-defined large-scale component is clearly present, antisymmetric with respect to the equatorial plane, and reaching here strengths of $\simeq 0.25\,\mathrm{T}$. This compares well to the simulation results of Browning *et al.* (2006; Fig. 2B), and supports their conclusion that a stably stratified tachocline-like layer is an essential component of a global solar-like large-scale dynamo.

Our ILES simulations break into novel territory in that they exhibit regular polarity reversals on multi-decadal time scales, something that to the best of our knowledge had not yet been observed in global 3D simulations of the SCZ operating in the turbulent regime. Figure 3 shows results of a low resolution simulation ($N_\phi \times N_\theta \times N_r = 128 \times 64 \times 47$) that was ran for almost 175 years. Figure 3A shows a time-latitude diagram of the zonally-averaged toroidal magnetic component extracted at the core-envelope interface in the simulation. Under the usual assumptions that sunspots do form following the buoyant rise and emergence of toroidal flux ropes formed and stored in the upper reaches of the tachocline, and that the number and the latitude of formation of these flux ropes are determined primarily by the strength of the large-scale toroidal magnetic field therein, this diagram is our simulation's analog to the well-known sunspot butterfly diagram.

Several features of this diagram are noteworthy: (1) the toroidal magnetic component undergoes fairly regular polarity reversals on a time scale of some 32 years. This is three times the observed mean period of the solar cycle, but the fact that the simulation yields a cycle at all is already remarkable; (2) the large-scale magnetic component manages to retain a dipole-like polarity pattern throughout the whole simulation interval, again in agreement with inferences based on sunspot magnetic polarities; (3) the deep-seated toroidal magnetic field is concentrated at mid-latitudes, rather than the lower latitudes indicated by the sunspot

butterfly diagram, but does show a hint of equatorward propagation in the course of each unfolding cycle; (4) despite strong fluctuations in the amplitude and duration of individual cycles, the two solar hemispheres manage to retain a good level of long-term synchronicity in their spatiotemporal evolution. These characteristics are all solar-cycle-like.

Figure 3B shows time series of the zonally-averaged toroidal magnetic flux density (B_T, solid lines) in each solar hemisphere, as color-coded, and of the polar cap radial magnetic flux density (B_P, dotted lines), again for each hemisphere. The former is calculated in a thin meridional slice straddling the core-envelope interface ($0.695 \leq r/R_\odot \leq 0.749$), and the latter at the top of the simulation domain over a cap extending 30 degrees in latitude from the poles. Despite strong temporal variability and marked amplitude and duration fluctuations from one cycle to the next, these time series leave no doubt as to the global and cyclic nature of the large-scale dynamo mechanism. The apparent predominance of positive-signed toroidal flux densities, independently of hemisphere, can be traced to the buildup of an equatorially concentrated band of positive toroidal field persisting from simulated cycle 2 to 4 and most prominent during simulated cycle 3 (see Figure 3A). The high degree of correlation between variations in the hemispheric polar cap fluxes indicates that the large-scale surface magnetic field is dominated by a dipole component approximately aligned with the rotation axis. Figure 3B also shows that the dipole moment and the deep-seated toroidal component oscillate essentially in phase.

Figure 3C shows a time-radius slice of the zonally averaged toroidal magnetic component, extracted at mid-latitudes in the Southern hemisphere. The cycles are seen to originate well within the SCZ, with the magnetic field undergoing further amplification once it has been pumped down into the underlying stably stratified fluid layer, reaching peak strengths in excess of 0.3 T for the stronger cycles. Field amplification also takes place in the upper half of the SCZ, but the toroidal field strength therein seldom exceeds 0.1 T. The signature of the magnetic cycle clearly pervades the whole SCZ.

4. The physical nature of the large-scale dynamo process

The simultaneous presence of a well-defined dipole moment and of a Reynolds-stress-driven axisymmetric mean differential rotation sustained throughout the simulation suggests that the simulation may be operating as what is known in mean-field theory as an $\alpha\Omega$ dynamo, with the regeneration of the poloidal magnetic component taking place through the agency of the so-called α-effect, more precisely, the $\alpha_{\phi\phi}$ component of the alpha tensor. For mildly inhomogeneous and mildly anisotropic fluid turbulence, the latter is predicted to be proportional to the negative flow helicity (cf., Ossendrijver 2003; Käpylä *et al.* 2006; and references therein). In our simulations the latter is predominantly negative in the Northern hemisphere, which should then yield a positive α-effect in the bulk of the SCZ. This is consistent with the production of a positive dipole moment from a toroidal component positive in the N-hemisphere, as seen on Fig. 3B.

It remains to be understood why our simulations manage to produce regular polarity reversals, while those of Browning *et al.* (2006) by all appearances do not. Both simulations are very similar in design, and reach comparable turbulent and magnetic intensities, at least judging from the convective flow speeds, strengths of mean magnetic field in stable layer, surface field strengths, ratio of total magnetic to kinetic energies, etc. However, our ILES approach allows to reach a highly turbulent state at relatively low spatial resolution, which in turn permits longer temporal integrations in reasonable wallclock time. It is certainly possible that the lack of polarity reversals in the Browning *et al.* (2006) simulations is a simple consequence of their relatively short integration time. The issue of so-called "spin-up" is also a possibility, as some of our simulations indicate that the time interval required to establish regular cyclic activity of the large-scale field is affected by the manner in which the simulation is initialized, although cyclic activity itself appears to be a robust feature.

The upper boundary condition may also play a role; Browning *et al.* (2006) match their simulated magnetic field to an exterior potential field, while our vertical-field boundary is probably more efficient at allowing magnetic helicity to exit the sim-

ulation domain, which is believed to favor large-scale dynamo action (cf., Käpylä *et al.* 2008; Brandenburg 2009; and references therein). At a more fundamental level, it is also quite possible that the behavior of the simulation at small spatial scales plays a key role in governing large-scale dynamo action. The latter can be viewed as a combination of forward and inverse cascades, of both magnetic energy and helicity, operating from the energy injection (intermediate) scale to both the (small) dissipative scales and the (large) dynamo scales. Varying treatment of the manner small scales are treated can affect the inverse cascades, especially if an insufficient separation of scales is realized in the simulation between the dissipative and energy injection scales. The numerical experiments of Elliott & Smolarkiewicz (2002) on purely hydrodynamical solar convection offer empirical support to this conjecture.

This letter has focused on the general characteristics of the solar-like cycles of the large-scale magnetic component building up in MHD implicit large eddy simulations of the solar convection zone. There are of course many additional simulation features that are of interest and need to be explored in detail. Our preliminary analyses indicate that low amplitude solar-like equatorially-propagating torsional oscillations develop across the convective envelope. We also detect a weak but clear signature of the magnetic cycle in the heat transport throughout the convective envelope. This has direct relevance to the ongoing debate regarding the ultimate origin of the observed decadal variations of the total solar irradiance during the activity cycle. We are currently investigating in detail these appealing features of our simulations.

The numerical simulations reported in this Letter were carried out primarily on the computing facilities of the Réseau Québécois de Calcul de Haute Performance. This work is supported by Canada's Natural Sciences and Engineering Research Council, Research Chair Program, and Foundation for Innovation (MG and PC). The National Center for Atmospheric Research is supported by the National Science Foundation (PKS).

REFERENCES

Brandenburg, A. 2009, SSRv, 144, 87.

Browning, M.K., Miesch, M.S., Brun, A.S., & Toomre, J. 2006, ApJ, 648, L157

Brun, A.S., Miesch, M.S., & Toomre, J. 2004, ApJ, 614, 1073

Cattaneo, F. 1999, ApJ, 515, L39

Charbonneau, P. 2005, LRSP, URL: http://www.livingreviews.org/lrsp-2005-2, accessed on 09.08.2005

Clune, T.L., Elliot, J.R., Glatzmaier, G.A., Miesch, M.S., & Toomre, J., 1999, Parallel Comput., 25, 361

Elliott, J.R., & P.K. Smolarkiewicz, P.K. 2002, Int. J. Numer. Meth. Fluids, 39, 855

Gilman, P. 1983, ApJS, 53, 243

Glatzmaier, G.A. 1984, J. Comput. Phys., 55, 461

Glatzmaier, G.A. 1985, ApJ, 291, 300

Goedbloed, H., Poedts, S. 2004, Principles of Magnetohydrodynamics, Cambridge University Press

Käpylä, P.J., Korpi, M.J., & Brandenburg, A. 2008, A&A, 491, 353

Käpylä, P.J., Korpi, M.J., Ossendrijver, M., & Stix, M.2006, A&A, 455, 401

Margolin, L. G., & Smolarkiewicz, P.K. 1998 SIAM J. Sci. Comput., 20, 907

Margolin, L. G., Rider, W. J. & Grinstein, F.F. 2006, J. Turb., 7, N15

Miesch, M.S., Elliott, J.R., Toomre, J., Clune, T.L., Glatzmaier, G.A., & Gilman, P.A. 2000, ApJ, 532, 593

Ossendrijver, M.A.J.H. 2003, A&AR, 11, 287

Piotrowski, Z.P., Smolarkiewicz, P.K., Malinowski, S.P., & Wyszogrodzki, A.A. 2009, J. Comput. Phys, 228, 6268

Priest, E.R., 2000, Solar magnetohydrodynamics, Kluwer Academic Publishers

Prusa, J.M., Smolarkiewicz, P.K., & Wyszogrodzki, A.A. 2008, Comp. Fluids, 37, 1193

Prusa, J.M., & Smolarkiewicz, P.K. 2003, J. Comput. Phys. 190, 601

Smolarkiewicz, P.K., Grubišić, V., & Margolin, L.G., 1997, Month. Weather Rev. 125, 647

Smolarkiewicz, P.K., Temperton, C., Thomas, S.J., & Wyszogrodzki, A.A. 2004, Proc. ECMWF Seminar Series, 6-10 September 2004, Reading, UK, 203

Smolarkiewicz, P.K., & Szmelter, J. 2009, J. Comput. Phys., 228, 33

Waite, M.L., & Smolarkiewicz, P.K. 2008, J. Fluid Mech., 606, 239

This 2-column preprint was prepared with the AAS LaTeX macros v5.2.